Luis Felipe-Sesé, Elías López-Alba, Francisco A. Díaz, Full-field 3D displacement and strain analysis during low energy impact tests employing a single-camera system, Thin-Walled Structures, Volume 148, 2020, 106584, ISSN 0263-8231, https://doi.org/10.1016/j.tws.2019.106584.

Full-field 3D Displacement and Strain analysis during low energy impact tests employing a single-camera system

Luis Felipe-Sesé[1*], Elías López-Alba[2], Francisco A. Díaz[2]

[1] Departamento de Ingeniería Mecánica y Minera, Campus Científico Tecnológico de Linares, Universidad de Jaén, 23700 Linares, Spain

[2] Departamento de Ingeniería Mecánica y Minera, Campus Las Lagunillas, Universidad de Jaén, 23071 Jaén, Spain

*Corresponding author: lfelipe@ujaen.es

Characterising materials behaviour during dynamics events such as impact require several features related to monitoring and instrumentation which find in full-field techniques one of the main responses due to high spatial and, nowadays, also temporal resolution. 3D-Digital Image Correlation has provided an interesting tool to evaluate the material response during impact testing. It contributes with displacement and strain fields at high frame rates, which represents enormous potential for subsequent analysis. However, 3D-DIC also presents some issues which may condition the experimentation. The first of them is the requirement of a stereoscopic optical system, which lead to important economic issues if high speed cameras are required. Secondly, certain impact arrangements have limited space which make complicated to dispose of a proper stereoscopic system observing an area of interest with a suitable angle that makes it possible r a successful processing. In this work, a recent procedure combining Fringe projection and 2D-DIC is presented as an alternative for impact testing analysis. As main characteristic, the optical arrangement is simplified to only one high speed camera and an additional simple LCD projector which makes it easier the experimentation, reducing significantly the setup cost. To demonstrate that capabilities of FP+2D-DIC as a simpler approach with results comparable to those obtained with 3D-DIC, in this work it was analysed 2, 3, 4, and 5mm thickness aluminium plates under low speed impacts with different energy levels. Impacts were performed employing an impact tower with a hemispherical impactor, connected to a load cell. During the impact, displacement and strain maps were measured at the non-impacted face of the specimen, using a single camera system implementing the combination of FP and 2D-DIC techniques. Permanent displacement and strain maps were validated with those obtained with a 3D-DIC system, supporting the potential of this FP+2D-DIC approach for impact testing.

1. Introduction

Characterising damage and mechanical behaviour of materials under impact presents some sensoring and instrumentation particularities which would benefit from using full-field techniques. As a highly versatile technique, 3D Digital Image correlation (3D-DIC) is commonly employed for this purpose [1–5]. This technique deals with stereo images for three-dimensional measurements, hence two cameras are needed. Specifically, in drop-weight impact tests, some authors considered 3D-DIC for different aims such as damage detection and evaluation. For instance, Lampeas and Pasialis [6] proposed an experimental methodology to validate nonlinear

dynamic simulations employing an impact tower. In fact, they evaluated the damage on the impacted face through 3D-DIC. However, impactor was an obstacle for cameras visualisation, considerably reducing the analysed area. To overcome this issue, alternatives based on mirrors are usually employed for measuring on the rear non-impacted surface [7–9]. Wang et al. [8] analysed the effect of different impact parameters on the damage and response of foam-core sandwich panels subjected to impact. Specifically, they arranged a mirror below the specimen which allowed a full-field analysis. A similar arrangement was employed by Pärnänen et al. [9] in their study of debonding in fibre metal laminates. 3D-DIC allowed full-field strain evaluation in the back surface by comparing reference and final deformed state images.

Despite that, 3D-DIC still presents some limitations related to the complexity of the set-up (two cameras could be complicated to be employed in reduced spaces) and facilities costs. Since measurement has to be performed on the non-impacted face, cameras positioning implies difficulty considering the available space and mirror location. Moreover, this limitation might lead to an excessive angle between the optical axis of both cameras, reducing the analysed area and even incurring projection errors. As alternative, Gulker et al. [10] studied the behaviour of composite plates using Fringe Projection (FP). Considering a simpler mirror arrangement, only a high speed camera is necessary, reducing the complexity of the set-up. In this case, out-of-plane displacement of the non-impacted face was determined during the test in a full-field manner. However, contrary to 3D-DIC, strains, which represent a fundamental magnitude to be determined for elastic, plastic and failure behaviour, were unable to be measured since in-plane displacements were unknown.

Moreover, combination of Fringe projection and 2D Digital Image Correlation (FP+2D-DIC) has been developed in the latest years looking for a low-cost system for full-field 3D measurement [11,12]. Fringe Projection (FP), based on Moiré effect, is a full-field optical technique that measures out-of-plane displacement usually employed for shape measurement. 2D Digital Image Correlation (2D-DIC) is a full-field optical technique to measure in-plane displacement, which corresponds with the displacement in a plane perpendicular to the optical axis, by tracking a grey random pattern known as speckle [13]. Similarities in the set-up, namely a camera perpendicular to the object, makes both techniques complementary, allowing 3D measurement. Different approaches have been developed for this integration, specifically in managing the superposition of the fringes and the speckle patterns, respectively necessary for FP and 2D-DIC, and the aberration of in-plane displacement measured when out-of-plane displacement also occurs [14,15]. One of the most important aspects in dynamic testing is the necessity of both patterns representing exactly the same instant in time. That restriction is satisfied by employing a colour camera and a colour encoding technique which has been adopted by some authors to discriminate both patterns, providing relevant advantages [16]. Based on the work of Siegmann et al. [11], Felipe-Sesé et al. [17] implemented a robust methodology for integration of FP+2D-DIC which considered the correction of virtual in-plane displacements generated due to out-of-plane ones [17] [18]. This methodology was employed for validation of numerical models [19] and study of vibration analysis [20,21] or preliminar dynamic tests [22]. Therefore, FP+2D-DIC is considered to be an interesting alternative to 3D-DIC considering that requires the same set-up employed by Gulker et al. [10] but it will overcome the lack of in-plane information, only including an speckle pattern on the region of interest.

In the present study, the capabilities of this technique characterising low-energy impact phenomenon (from 1 to 25J) are explored. Aluminium plates with different thickness (2, 3, 4 and 5 mm) were tested under different impact energies using a Drop-Weight Impact Tower (DWIT) and a hemispherical impactor. A colour high speed camera was employed to register the deformation process. Besides full-field displacements, full-field strains were determined during the impact. Time evolution of the maximum displacement using FP+2D-DIC were analysed together with the experienced displacement of the impactor, obtained by double integration of

the load cell force signal [10,23]. Final shape and remaining strains on surface of plates was subsequently determined using 3D-DIC for validation purposes. To evaluate the similarity of both techniques, comparative is based on image decomposition, specifically on an analysis of the coefficients of Tchebichef moment descriptors.

2. Experimental Procedure

The aim was to analyse the strain fields along the impact on aluminium plates and how the thickness of the plate affects to the deformation of specimens at different energy rates. For that purposes, this section described the experimental methodologies and arrangements employed based on previous description of techniques.

2.1 Measuring technique

Fringe projection (FP) is based on projecting parallel fringes on the specimen surface to determine the out-of-plane shape changes. This structural light pattern should be obliquely projected to exhibit an in-plane displacement when the specimen experiences 3D displacement. Moreover, 2D-DIC is a full-field optical technique for measuring *X*- and *Y*- displacements [24]. It is a light-intensity-based technique which relies on the use of digital image processing. In this technique, areas of recorded images are grouped into virtual sets of pixels called facets which are tracked in subsequent images when displacement occurs.

Drop weight impacts usually generate large out-of-plane displacements and significant in-plane displacements. This implies the need to measure surface displacements in all three dimensions simultaneously during the dynamic loading. This is the reason why in this study a combined fringe projection (FP) [25] and two-dimensional digital image correlation method (2D-DIC) [24] was utilised based on earlier work [17,18,26].

Hence, the integration method FP+2D-DIC employs a conventional LCD projector and a colour RGB high-speed camera. Every single RGB colour images can be decomposed into three, each of them are sensitive to red, green or blue colour spectrums, this feature allow the independent processing of fringe and speckle patterns. The projector is used to create a blue and white fringe pattern with a sinusoidal intensity profile on the measured surface which permits FP analysis to be performed in the red colour image, obtaining out-of-plane shape map. In addition, a red speckle pattern on a white background is sprayed onto the measured surface letting two-dimensional digital image correlation to be performed in the blue spectrum image.

Images of the measured surface were captured before, as a reference state, and during the impact using the high-speed RGB camera. Speckle pattern was processed using a commercial digital image correlation algorithm (VIC 2D from Correlated Solutions Inc.). Moreover, fringe pattern information was processed using Fourier Transform Profilometry [25] combined with a quality unwrapping algorithm[27].

Since a telecentric lens was not employed, the measured in-plane displacements from the digital image correlation were distorted by the out-of-plane displacements [14,15,28]. Hence, to perform a correct quantification, measured in-plane displacements were corrected using the out-of-plane displacements measured using the fringe projection system according to Eq (1) .

$$\begin{cases} \Delta x = L\left[\Delta x_{CCD} - \left(x_{2,CCD}\dfrac{\Delta z_2}{z_0} - x_{1,CCD}\dfrac{\Delta z_1}{z_0}\right)\right] \\ \Delta y = L\left[\Delta y_{CCD} - \left(y_{2,CCD}\dfrac{\Delta z_2}{z_0} - y_{1,CCD}\dfrac{\Delta z_1}{z_0}\right)\right] \end{cases} \quad \text{Eq (1)}$$

Where $(x_{1,CCD}, y_{1,CCD})$ and $(x_{2,CCD}, y_{2,CCD})$ are the initial and final position respectively of each element surface represented in the image by a pixel; Δz_1 and Δz_2 are the corresponding out-of-plane position in initial and final position at corresponding pixel; z_0 is the distance between the reference surface and the optical centre of the camera lens and L is the inverse of the lateral magnification (in millimetre per pixel units) at z_0 distance. This correction methodology had been developed previously [17] and is based on a pin-hole model o lenses. Additionally, a calibration procedure was used to align the optical axis of the camera perpendicular to a plane reference surface and to obtain the distance from the reference surface to the camera z_0 [18].

As previously shown, impacted plates experiences large displacements during contact experiments. FP-DIC technique measures only displacement and strain should be calculated in post-processing. Additionally, the classic formulation for strain based on Cauchy strain tensor is not valid for this particular analysis where large displacements could occur. To overcome this issue an extended formulation based on Lagrange strain tensor [29] was implemented to achieve strain maps from FP+2D-DIC displacement maps according to the following equations.

$$\varepsilon_{xx} = \frac{\delta\Delta x}{\delta x} + \frac{1}{2}\left[\left(\frac{\delta\Delta x}{\delta x}\right)^2 + \left(\frac{\delta\Delta y}{\delta x}\right)^2\right] \quad \text{Eq (2)}$$

$$\varepsilon_{yy} = \frac{\delta\Delta x}{\delta y} + \frac{1}{2}\left[\left(\frac{\delta\Delta x}{\delta y}\right)^2 + \left(\frac{\delta\Delta y}{\delta y}\right)^2\right] \quad \text{Eq (3)}$$

$$\gamma = 2\varepsilon_{xy} = \frac{\delta\Delta y}{\delta x} + \frac{\delta\Delta x}{\delta y} + \frac{\delta\Delta y}{\delta x}\frac{\delta\Delta y}{\delta y} + \frac{\delta\Delta x}{\delta x}\frac{\delta\Delta x}{\delta y} \quad \text{Eq (4)}$$

2.2 Image Decomposition

Validation of the results obtained with FP+2D-DIC was performed by comparing its results with those obtained with 3D-DIC. Namely, this procedure consisted on analysing the plate with 3D-DIC after the impact and compare the displacement and strains fields with those obtained with FP+2D-DIC at the end of the test when the impactor released the plate.

Size and orientation of strain and displacement maps may be different between techniques since they present different optical set-up, hence Image Decomposition method, which is independent to those parameters [30–32], was employed to compare them. This method is widely employed for validation of analytical and theoretical models [31]. Its fundamentals consists in transform the information from each displacement or strain maps, obtained by each technique, into respective feature vectors which can be directly compared. Using this approach, it is possible to eliminate the influence of the images size and camera view angles, making it possible to perform a direct comparison of the results.

The adopted image decomposition method was based on Tchebichef polynomials $\tilde{T}(i,j)$ [32–34] to decompose displacements images I*(i,j)* into units of mm.

$$I(i,j) = \sum_{i=1}^{N} f_i \widetilde{T}_i(i,j) \quad \text{Eq (5)}$$

Where f_i is the ith Tchebichef moment and is the $\widetilde{T}_i$ scaled 2D Tchebichef polynomials, i.e. the magnitude is f_i and $\widetilde{T}_i$ gives the normalized shape. *N* is the number of shape descriptors selected also called moments. The complete number of descriptors could be up to $(N_r \cdot N_s)$ x 1 being N_r and

N_s the number of rows and columns of the image. More information about the decomposition procedure could be found in the work performed by W. Wang et al. [34].

Polynomials are dimensionless and, hence, units will be those of the decomposed data map. The required number of shape descriptors is given by the achievement of a proper correlation coefficient between the original and the reconstructed image using *N* shape descriptors[35]. To perform this decomposition, Euclid V1.01 software has been employed [36].

2.3 Experimental set-up

One of the main components to perform commented impact tests was the Drop-Weight Impact Tower (DWIT) where a hemispheric projectile impacted the specimen with different energies. The total mass of the impacting system (consisting on guide arrangement, load cell and projectile) was 7.21 kg. This mass was positioned at different heights to achieve different levels of impact energy. Specifically, the projectile consisted on a perfectly rigid steel component (where it is assumed that no deformation is experience during the tests) of a diameter of 8mm connected to a HBM CFT 20kN load cell to record the load of impact.

As commented previously, the subjects of study were 150x150 specimens of 2, 4, and 5mm thick made from Aluminium 1050. They were horizontally clamped along the perimeter, leaving a free area of 120 × 120 mm on the testing area as presented in Figure 1.

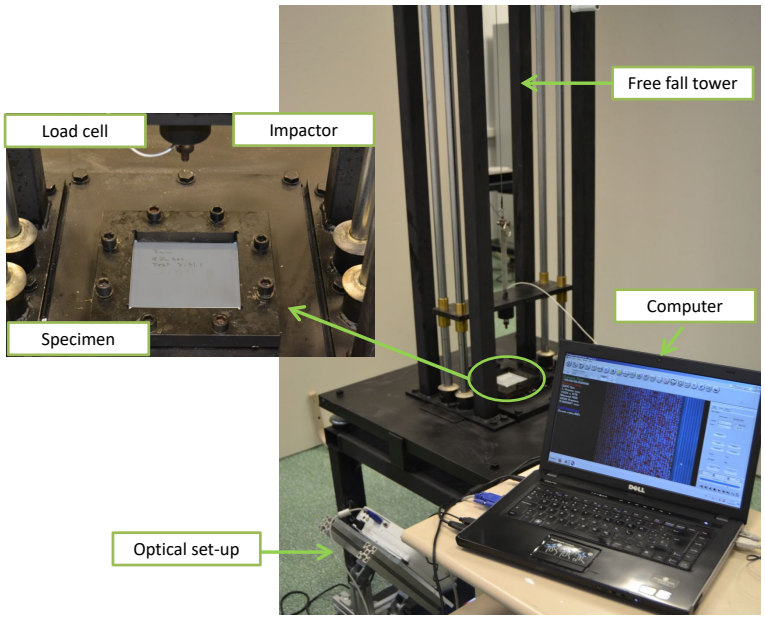

Figure 1 Impact test set-up

The experimental optical set-up required to accomplish this study presented some particularities briefly advanced in the introduction section. Obviously the impacted side of the specimen was not possible to be analysed during the impact and, hence, the focus of the optical analysis was placed on the underside as observed in Figure 1 .

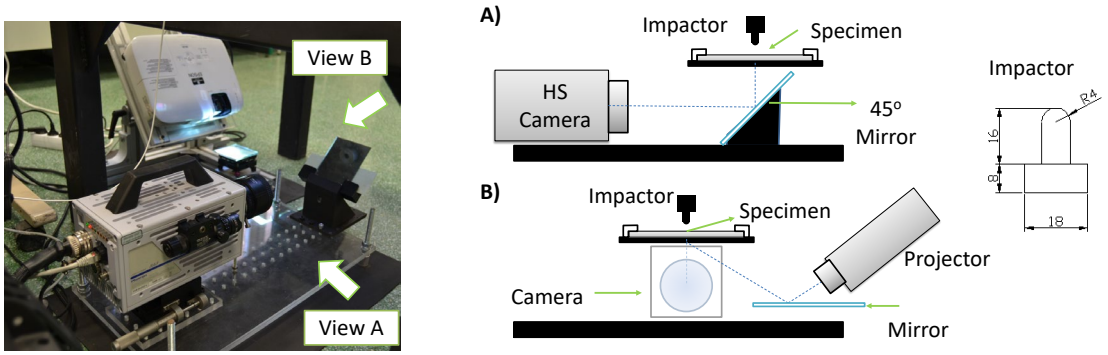

Figure 2 Image of Optical set-up (left). A) Schematic illustration of camera system. B) Schematic illustration of projection system

Due to space requirements and horizontality of the specimen, a system of first-surface-mirrors was strategically disposed at 45° in order to observe the region of interest with a high speed camera placed horizontally and recording at 3000 fps. Specifically, it was a Photron FASTCAM SA3 model 120K-C1 with 85mm focal length Nikon lenses and a resolution of 1024x576 pixels, which leaded to a lateral optical magnification of 0.145mm/px. Load cell signal was synchronized with the camera clock, so, for each captured image, there was a sample of the load cell. In addition, fringes were obliquely projected on the region of interest. Previous space consideration also conditioned this aspect and the projector (EPSON EB-U32) was arranged to project on the specimen through the reflexion on a first surface mirror. These elements were adjusted in order to find a balance between projection angle and reduced shadow on the specimen as observed in Figure 3. However, the presence of shadow on specimen is not a limitation due to the symmetric behaviour of the plates under test conditions. Also in that figure it is presented the analysed region of interest limited by green dashed lines and the centred impact point marked by a cross. Speckle Images were processed using a 2D-DIC commercial software package (by Correlated Solutions Inc.) with a 27 pixel facet and 1 pixel overlap to maintain the same image size as FP results.

Calibration of this optical set-up was performed following the procedure developed in previous work [18,37]. According to that procedure, camera and projector set has to be displaced a certain distance Δz along optical axis, capturing fringe pattern images at z_0 and $z_0+\Delta z$ distances. Those images are processed obtaining a difference in the phase of projected fringe patterns ($\Delta\varphi$) which can be related with the Δz value obtaining the required K factor in mm/radians units to obtain Z maps from Diphase maps. Nevertheless, in this case, camera and projector were placed in independent mountings which implied some limitations for displacing both in a synchronized and controlled manner. However, the calibration of FP+2D-DIC is versatile, consequently, instead of displace the optical set-up, a calibration plate was simply micrometrically displaced between a z_0 distance and a distance z_0+5mm. Images at those two stages were captured and calibration was performed. Since no other displacement but that Δz 5mm was accomplished, the analysis of the *X*-, *Y*- and *Z*- displacements measured during calibration process gave an indication of the uncertainty of the measurement. This was calculated as the standard deviation of the *Y*- and *Z*- displacements fields considering that actual displacement maps were homogenous of 0 and 5 mm respectively. In this case, uncertainties of 0.018mm and 0.09mm for in and out-of-plane displacement were respectively obtained.

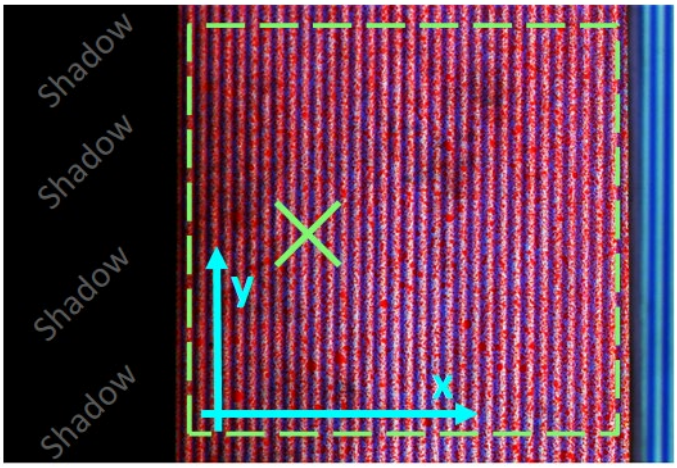

Figure 3 Image captured with optical set-up showing the specimen with speckle pattern and projected fringe pattern. Reference coordinate system is represented by cyan axes. Dashed green line highlight the analysed region of interest and green cross indicates impact point.

3. Results

Specifically, it was performed four different energy level tests on the four different thicknesses plates. Table 1 presents an outline of the different levels of energy tested depending on the plate thickness. Since sixteen data sets (consisting in three displacement and two strain maps together to load cell data) are a large quantity of results, they will be summarized in different illustrative figures and graphs.

Plate thickness	2mm	3mm	4mm	5mm
Energy Tested	1 J	4 J	4 J	8 J
	2 J	6 J	8 J	12 J
	3 J	8 J	12 J	16 J
	4 J	10 J	16 J	25 J

Table 1 Impact test performed as function of thickness

In Figure 4 it is presented the maximum (top row) and permanent (bottom row) out-of-plane, i.e. *Z*- direction, displacement measured along the maximum energy tests for 2, 3, 4 and 5 mm thicknesses and 4, 10, 16 and 25 J respectively. It is observed some tendency to recover the original shape due to elastic behaviour once the indenter is not in contact with the specimen. However, the high ductility of this Aluminium 1050 allow high plasticity and permanent deformation which is observed in all the tests and elastic recovery is mainly produced due to bending mechanism. To easily observe the evolution of out-of-plane displacement as energy increases, Figure 5 shows that evolution along black dashed profile of Figure 4. For all the analysed cases, it is observed similar profile evolutions. The influence of thickness and energy is remarkable in these tests. When the energy employed is the same but different thicknesses are tested bending effect is highlighted. For example, for 2 and 3 mm thickness with an energy of 4 J, it is observed that maximum out-of-plane displacement are 4.01 and 2. 75 mm respectively. This implies that bending is more prominent when it is tested thinner plates, as expected since the inertia moment is increased. Similar results are obtained, comparing 8 J energy in 3, 4 and 5 mm thick. The maximum out of plane displacements obtained in those cases were 4.02, 2.50 and 2.04 mm. Similar results are observed for tests at 12 J in 4 and 5 mm thickness and 16 J for

4 and 5 mm thickness plates. In all cases, some noise is present as remanence of speckle pattern on fringe pattern.

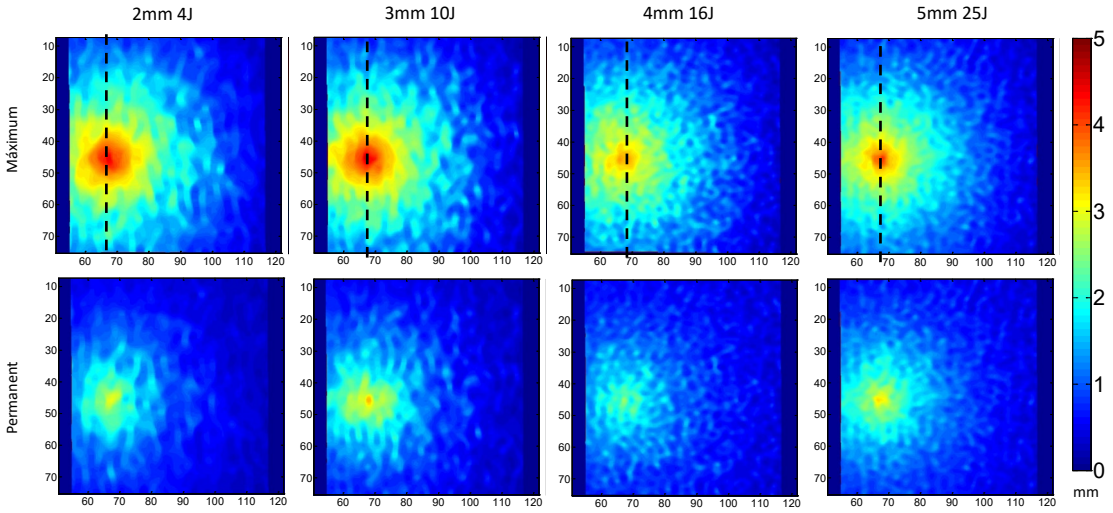

Figure 4 Maximum (upper row) and permanent (down row) out-of-plane displacement measured at maximum energy tests in the four different plates.

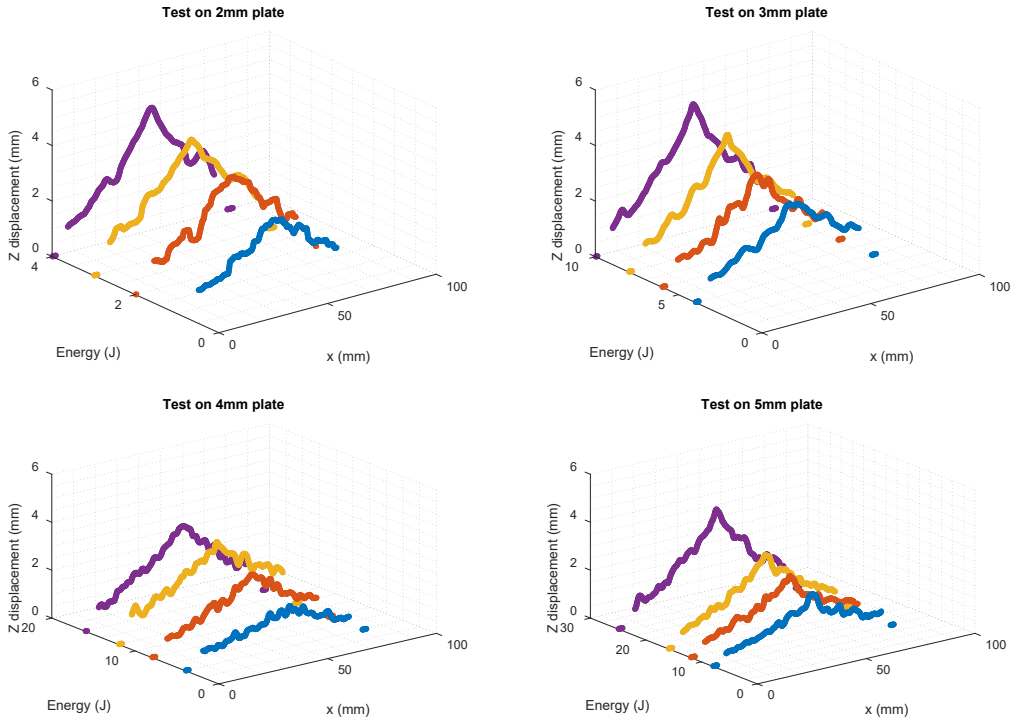

Figure 5 Evolution of out-of-plane displacement along vertical profile of Figure 4 with impact energy and different thickness plate.

Displacement measured in the contrary to impact surface by FP+2D-DIC is compared with that calculated by integration of the signal measured by the load cell as observed in Figure 6. As noticed, displacement signal from load cell was recorded slightly earlier than optical measurement of the rear surface. The reason is because simultaneously to bending mechanism is produce indentation in the specimen. This deformation is experienced first in the front face where the indenter impact with the specimen. In addition, displacement measured in the upper face is slightly higher that obtained in the lower surface, which means thickness reduction in the specimen due to indentation mechanism. This effect is observed in Figurer 6, when the thickness increase, the differences between the maximum displacements provided by the load cell and

the rear face of the specimen increase. That is, the difference in displacement of both sides of the plates differs with energy and thickness due to indentation of the projectile. This means that thicker specimens experience less bending during the impact and therefore more indention is produced in the plates [38].

In next Figure 7, it is presented those differences of displacement (indentation) measured for all the tests performed. All of them show a clear dependency on thickness and energy. For instance, difference for 1J impact on 2mm thickness plate is negligible, and however, the difference will reach 1.15mm for 25J test on 5mm plate. This lead to the fact that indentation in the plate directly increases with those two factors.

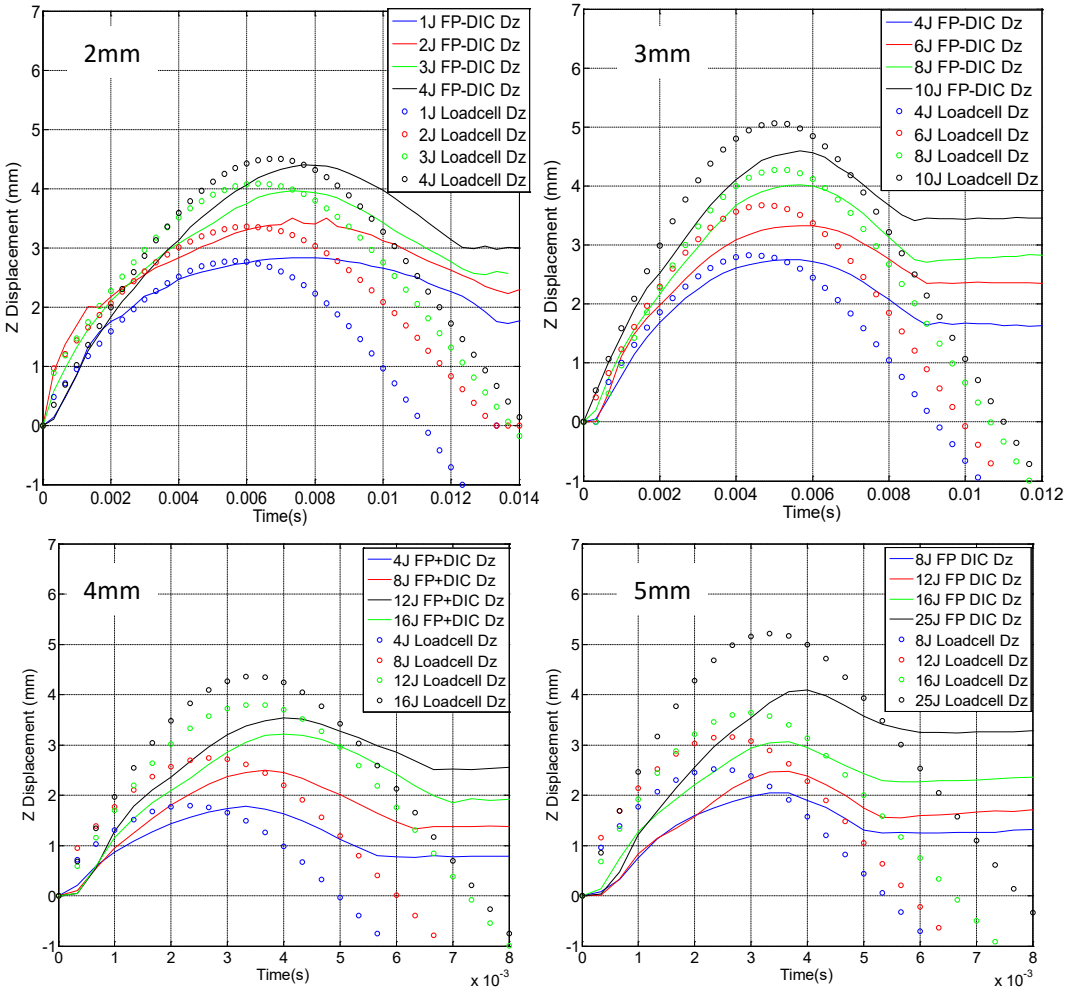

Figure 6 Out-of-plane displacement measured by FP+2D-DIC together with measured obtained from load cell signal.

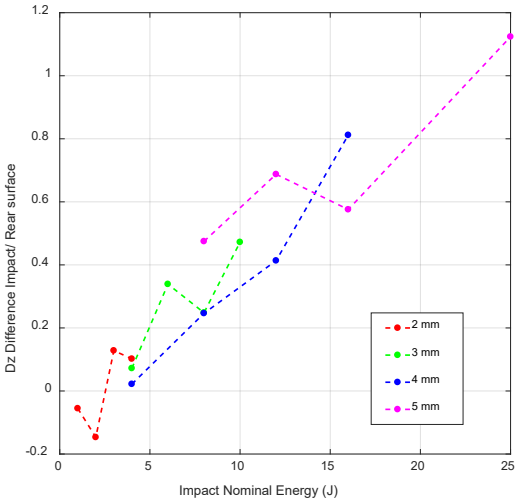

Figure 7 Evolution of the difference of Z- Displacement between upper and lower Surface with plate thickness and impact energy.

The capabilities of the proposed optical system are also illustrated with an additional post-processing analysis conducted based on next Figure 8. On it, it is plotted load results versus out–of-plane displacement in the rear face of specimens, specifically, where the maximum displacement is measured. The area under the loading branch is the energy employed to deform the specimen under bending considerations, while the area under the unloading branch is the recovered elastic energy. Hence, the difference between both areas results in the absorbed energy to produce permanent deformation and is specified on the legend of each plot, that is, the energy employed for permanent flexure deformation.

It is observed that, in terms of percentage, no big differences exists and the main absorbed energy due to bending effect is 86.5% respect to the potential energy.

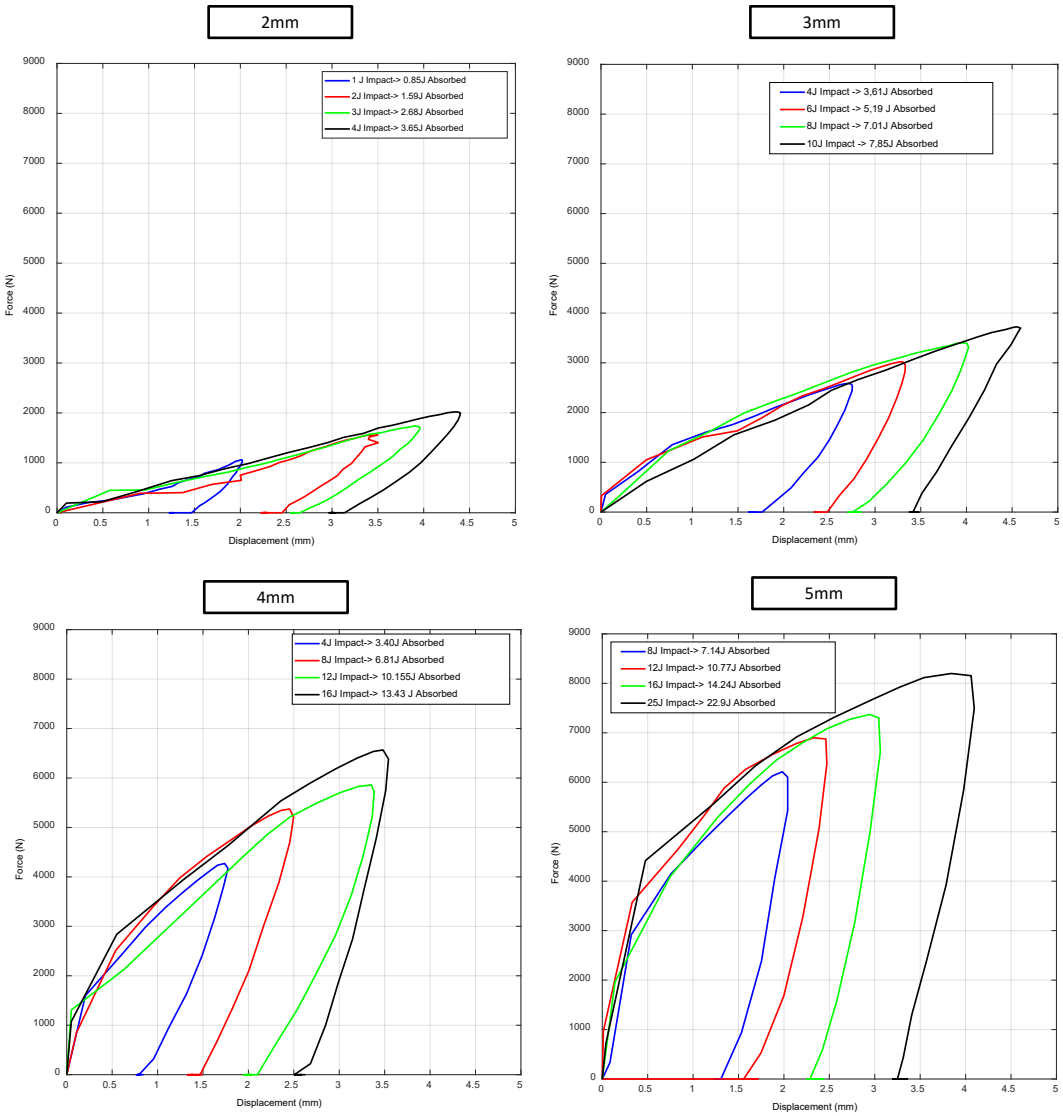

Figure 8 Force versus displacement experienced in the rear surface (at impact point) providing energy loops for tests performed in aluminium plates from 2 to 5mm thickness.

In addition, as mentioned at the beginning, one of the main interests of employing FP+2D-DIC in these tests, and one of the main novelties of this work, is the possibility of measuring in-plane strain. To demonstrate this capability,Figure 9 shows ε_{xx}, ε_{yy}, and ε_{xy} strain maps of a certain instant during a 10 J impact test, in fact the maximum force instant.

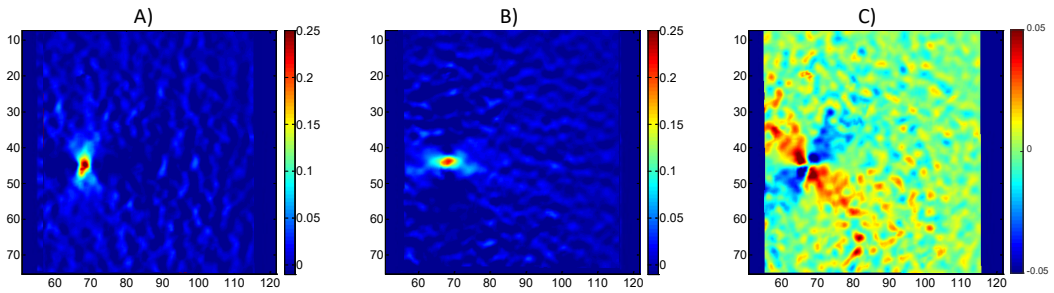

Figure 9 Strain maps representing A) ε_{xx}, B) ε_{yy}, and C)ε_{xy} in a 3mm thickness plate at maximum strain during a 10 J impact

As observed, since the impact is centred and it exists symmetry in the specimen and clamping, ε_{xx} and ε_{yy}, are similar but rotated ninety degrees. Hence, the following presentation of results will be focused in ε_{yy} to reduce the number of strain maps presented and ease its understanding. Figure 10 represents strain maps according to same intents as in Figure 5, i.e., instant with maximum strain and final permanent ε_{yy} strain.

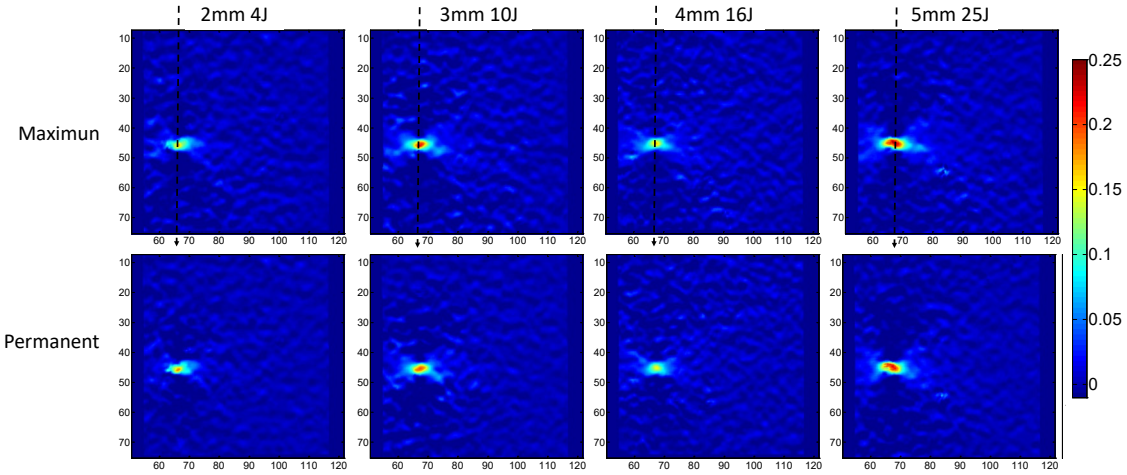

Figure 10 Maximum (upper row) and permanent (lower row) ε_{yy} strain measured for each plate thickness.

To observe the evolution of strains in detail, next figure shows the evolution of the strain with time along vertical profile highlighted by a black dashed line in Figure 9, which is similar to the one in Figure 4.

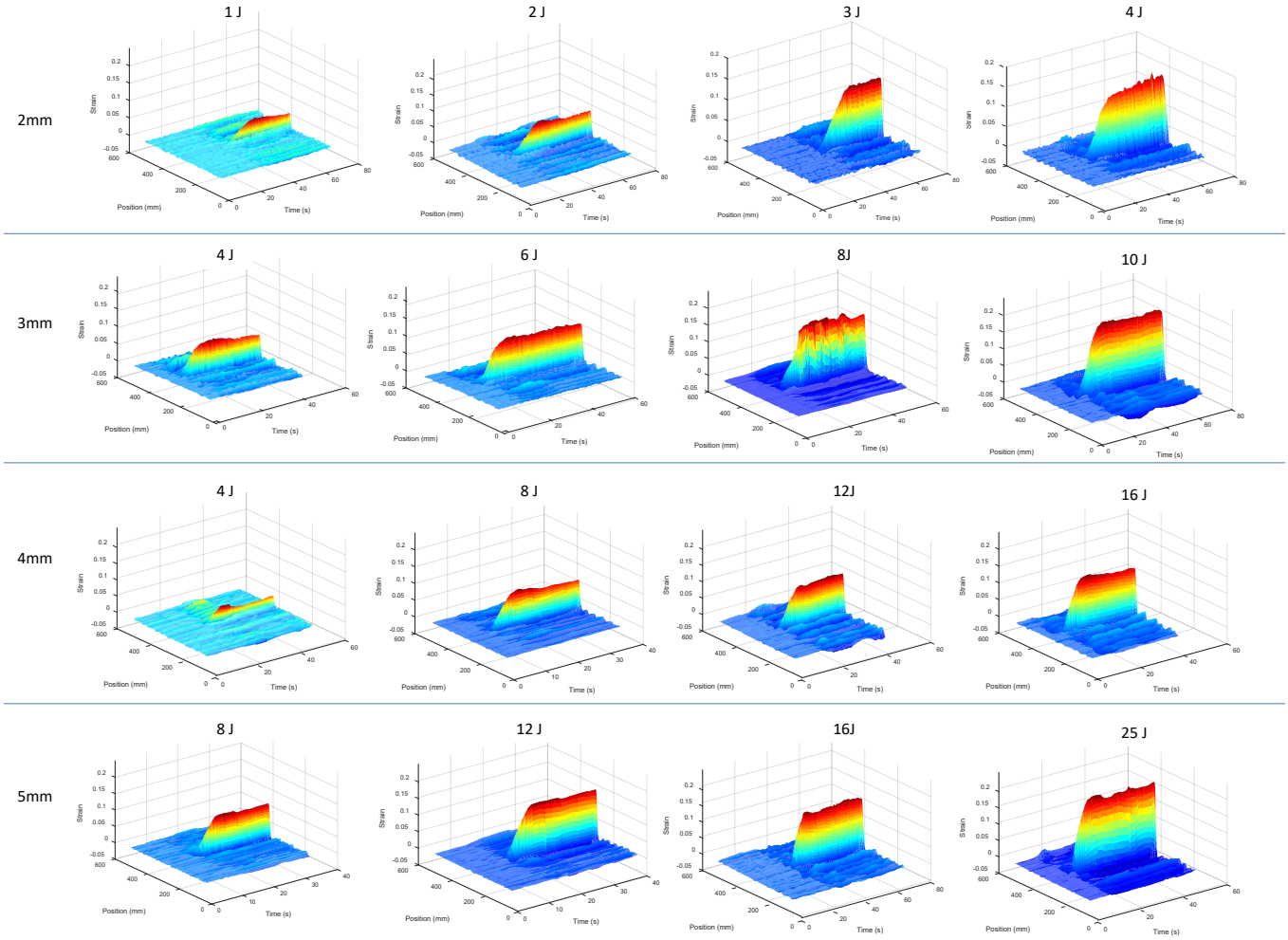

Figure 11 Evolution of strain along profile of Figure 9 with time in the sixteen different tests

In Figure 9 and Figure 10, it is shown a general trend in which main component of strain is permanent, i.e. plastic strain. Negligible strain is recovered after releasing of the impactor. This is consistent with previous analysis of maximum and permanent *Z*- Displacements, which again is rely on the characteristics of high toughness and ductility of this Aluminium 1050 [39–41].

4. Validation of the methodology

The validation of the measurements performed using FP+2D-DIC exposed in previous section has been performed by comparing the permanent displacements maps and strains with those measured with 3D-DIC. For that purpose, before and after performing the impact test, each plate was placed on a specific rig where two sets of images were captured respectively with 3D-DIC system as observed in Figure 11. Set-up was composed by two Allied Stingray Cameras with 1032x776pixels and 25mm focal length lenses which offered a magnification of 0.169 mm/pixel. Accuracy of the system would be ±0.015 pixels (0.0025mm for this set-up) and ±100 με for surface strains according to previous studies [13]. As commented previously, image decomposition was employed to make the comparative possible. Specifically, each strain and displacement fields were decomposed into 100 Tchebichef shape descriptors in order to achieve a correlation coefficient higher than 90% between original and reconstructed displacement maps or field [32][35].

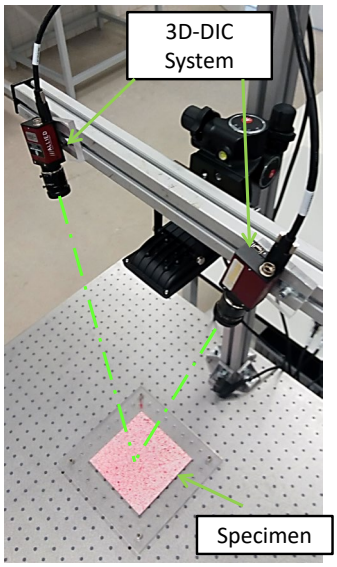

Figure 12 Validation set-up

The sets of shape descriptors (SD) describing each field from each test were treated as feature vectors. This vectors obtained from both experimental techniques were compared using the Euclidean distance between them, that is the SD difference. Euclidean distance is simply the straight-line distance between the locations represented by the vectors in multi-dimensional space, so that two coincident vectors would have a Euclidean distance of zero. The evolution of the Euclidean distance between the feature vectors representing the displacement and strain maps from 3D-DIC and FP+2D-DIC are shown in Figure 12 for each test.

As observed for each direction of displacement, differences increases with the level of energy of impact. However, heeding previously commented levels of uncertainty obtained from calibration procedure, it is noticed that level of difference in out-of-plane displacements in Figure 12 are compatible with cited uncertainties. That uncertainty could be improved by increasing the angle of the projected fringes, however, that would involve an increase in the shadow observed in Figure 3, being a drawback for a proper analysis.

Moreover, attending to in-plane SD differences, the maximum dissimilarity could be converted into pixel units by applying magnification factor of lenses, which lead to a maximum difference of 0.345 pixels, a subpixel value which a really reasonable difference.

In terms of percentage respect to maximum measured permanent value, it is observed that differences are always below 7.7% for out-of-plane displacement maps and below 2% for strain maps.

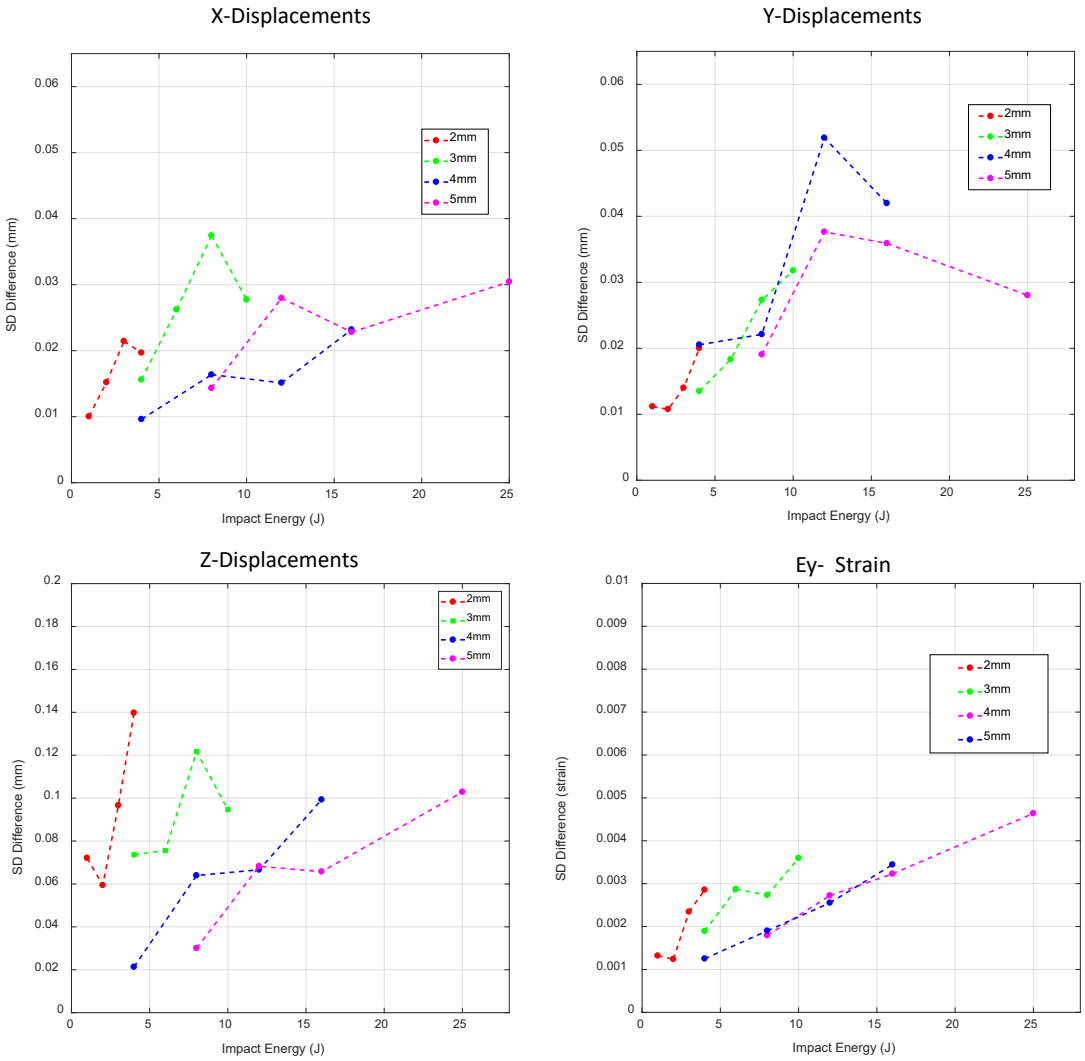

Figure 13 Evolution off Euclidean distance between feature vectors of 3D-DIC and FP+DIC for X-displacements (A), Y-displacements (B), Z-displacements (C) and ε_{yy} stains (D)

5. Conclusions

In this work, it has been evidenced that the proposed optical system allows obtaining high definition 3D displacement and strains maps with a single camera under dynamic conditions. That will ease the successfully realization of further integrity analyses of components submitted to impact solicitations.

Leading by example, it has been successfully performed full-field analysis of 2, 3, 4, and 5mm thickness aluminium plates under different impact energies solicitations using an impact tower and FP+2D-DIC results offered high potential. Specifically, it was observed that the main components of maximum strains were composed by plastic strains, being negligible the elastic strain components, due to high concentration of the solicitation and the high toughness of the material. However, some recuperation was also observed in *Z*- displacements, which was mainly due to bending solicitation component. Related to that, energy absorbed due to flexure solicitation was also possible to be quantified for each of the performed tests.

It was additionally observed the evolution of the importance of the indentation effect as the thickness of the specimen increased by comparing the displacement from both sides of the specimens. That could help for future investigations about thin and thick plate behaviour.

Moreover, measurements have been validated by comparing permanent displacement and strain maps with 3D-DIC by the use of Image Decomposition. Results endorse the capabilities of FP+2D-DIC for impact testing, highlighting the high similarities obtained for in-plane results of displacements and strain with differences lower to 2%.

In conclusion, FP+2D-DIC has been exploited for first time for impact analysis stablishing a new straightforward facility for the investigation of not only displacement in the three spatial direction but, additionally, strains with a high spatial resolution.

6. References

[1] J. Liu, D. Saletti, S. Pattofatto, H. Zhao, Impact testing of polymeric foam using Hopkinson bars and digital image analysis, Polym. Test. 36 (2014) 101–109. doi:10.1016/j.polymertesting.2014.03.014.

[2] P. Kumar, J. LeBlanc, D.S. Stargel, A. Shukla, Effect of plate curvature on blast response of aluminum panels, Int. J. Impact Eng. 46 (2012) 74–85. doi:10.1016/j.ijimpeng.2012.02.004.

[3] C.A. Featherston, J. Mortimer, M.J. Eaton, R.L. Burguete, R. Johns, The Dynamic Buckling of Stiffened Panels –A Study Using High Speed Digital Image Correlation, Appl. Mech. Mater. 24–25 (2010) 331–336. doi:10.4028/www.scientific.net/AMM.24-25.331.

[4] F. Pierron, M.A. Sutton, V. Tiwari, Ultra High Speed DIC and Virtual Fields Method Analysis of a Three Point Bending Impact Test on an Aluminium Bar, Exp. Mech. 51 (2011) 537–563. doi:10.1007/s11340-010-9402-y.

[5] V. Tiwari, M.A. Sutton, S.R. McNeill, S. Xu, X. Deng, W.L. Fourney, D. Bretall, Application of 3D image correlation for full-field transient plate deformation measurements during blast loading, Int. J. Impact Eng. 36 (2009) 862–874. doi:10.1016/j.ijimpeng.2008.09.010.

[6] G.N. Lampeas, V.P. Pasialis, A hybrid framework for nonlinear dynamic simulations including full-field optical measurements and image decomposition algorithms, J. Strain Anal. Eng. Des. 48 (2013) 5–15. doi:10.1177/0309324712462657.

[7] M.K. Hazzard, S. Hallett, P.T. Curtis, L. Iannucci, R.S. Trask, Effect of Fibre Orientation on the Low Velocity Impact Response of Thin Dyneema® Composite Laminates, Int. J. Impact Eng. 100 (2016) 35–45. doi:10.1016/j.ijimpeng.2016.10.007.

[8] J. Wang, A.M. Waas, H. Wang, Experimental and numerical study on the low-velocity impact behavior of foam-core sandwich panels, Compos. Struct. 96 (2013) 298–311. doi:10.1016/j.compstruct.2012.09.002.

[9] T. Pärnänen, A. Vänttinen, M. Kanerva, J. Jokinen, O. Saarela, The Effects of Debonding on the Low-Velocity Impact Response of Steel-CFRP Fibre Metal Laminates, Appl. Compos. Mater. 23 (2016) 1151–1166. doi:10.1007/s10443-016-9505-4.

[10] B. Gulker, R. Lureau, D. Liu, Investigation of Impact Response of Composites with Projection Moiré Enhancement, Exp. Mech. 54 (2014) 35–43. doi:10.1007/s11340-012-9677-2.

[11] P. Siegmann, V. Álvarez-Fernández, F. Díaz-Garrido, E. a Patterson, A simultaneous in- and out-of-plane displacement measurement method., Opt. Lett. 36 (2011) 10–12. doi:10.1364/OL.36.000010.

[12] C. Mares, B. Barrientos, a Blanco, Measurement of transient deformation by color encoding., Opt. Express. 19 (2011) 25712–25722.

[13] H. Schreier, J.-J. Orteu, M.A. Sutton, Image Correlation for Shape, Motion and Deformation Measurements, Springer US, Boston, MA, 2009. doi:10.1007/978-0-387-78747-3.

[14] C.J. Tay, C. Quan, T. Wu, Y.H. Huang, Integrated method for 3-D rigid-body displacement measurement using fringe projection, Opt. Eng. 43 (2004) 1152. doi:10.1117/1.1687728.

[15] C.J. Tay, C. Quan, Y.H. Huang, Y. Fu, Digital image correlation for whole field out-of-plane displacement measurement using a single camera, Opt. Commun. 251 (2005) 23–36. doi:10.1016/j.optcom.2005.02.070.

[16] C. Mares, B. Barrientos, a Blanco, Measurement of transient deformation by color encoding., Opt. Express. 19 (2011) 25712–22. http://www.ncbi.nlm.nih.gov/pubmed/22273963.

[17] L. Felipe-Sesé, P. Siegmann, F.A. Díaz, E.A. Patterson, Simultaneous in-and-out-of-plane displacement measurements using fringe projection and digital image correlation, Opt. Lasers Eng. 52 (2014) 66–74. doi:10.1016/j.optlaseng.2013.07.025.

[18] L. Felipe-Sesé, P. Siegmann, F.A. Díaz, E.A. Patterson, Integrating fringe projection and digital image correlation for high-quality measurements of shape changes, Opt. Eng. 53 (2014). doi:10.1016/j.optlaseng.2013.07.025.

[19] L. Felipe-Sesé, F.A. Díaz, E.A. Patterson, Exploiting measurement-based validation for a high-fidelity model of dynamic indentation of a hyperelastic material, Int. J. Solids Struct. (2016). doi:10.1016/j.ijsolstr.2016.06.036.

[20] L. Felipe-Sesé, F.A. Díaz, Damage methodology approach on a composite panel based on a combination of Fringe Projection and 2D Digital Image Correlation, Mech. Syst. Signal Process. 101 (2018) 467–479. doi:10.1016/j.ymssp.2017.09.002.

[21] L. Felipe-Sesé, Á.J. Molina-Viedma, E. López-Alba, F.A. Díaz, FP + DIC for low-cost 3D full-field experimental modal analysis in industrial components, 128 (2019) 329–339. doi:10.1016/j.ymssp.2019.04.004.

[22] L. Felipe-Sesé, E. López-Alba, P. Siegmann, F.A. Díaz, Integration of fringe projection and two-dimensional digital image correlation for three-dimensional displacements measurements, Opt. Eng. 55 (2016) 121711. doi:10.1117/1.OE.55.12.121711.

[23] O.S. David-West, D.H. Nash, W.M. Banks, An experimental study of damage accumulation in balanced CFRP laminates due to repeated impact, Compos. Struct. 83 (2008) 247–258. doi:10.1016/j.compstruct.2007.04.015.

[24] B. Pan, K. Qian, H. Xie, A. Asundi, Two-dimensional digital image correlation for in-plane displacement and strain measurement : a review, Meas. Sci. Technol. 20 (2009) 1–17. doi:10.1088/0957-0233/20/6/062001.

[25] M. Takeda, H. Ina, S. Kobayashi, Fourier-transform method of fringe-pattern analysis for computer-based topography and interferometry, J. Opt. Soc. Am. 72 (1982) 156. doi:10.1364/JOSA.72.000156.

[26] L. Felipe-Sesé, F.A. Diaz-Garrido, E.A. Patterson, Exploiting measurement-based validation for a high-fidelity model of dynamic indentation of a hyperelastic material, Int. J. Solids Struct. 97_98 (2016) 520–529. doi:10.1016/j.ijsolstr.2016.06.036.

[27] D. Ghiglia, M. Pritt, Two-dimensional phase unwrapping: theory, algorithms, and software, 1998. doi:10.1177/004057368303900411.

[28] C. Quan, C.J. Tay, Y.H. Huang, 3-D deformation measurement using fringe projection and digital image correlation, Opt. - Int. J. Light Electron Opt. 115 (2004) 164–168.

doi:10.1016/S0030-4026(08)70004-4.

[29] X.. b Tan, Y.. Kang, E.. Patterson, An experimental study of the contact of a rounded rigid indenter with a soft material block, J. Strain Anal. Eng. Des. 49 (2014) 112–121. doi:10.1177/0309324713496406.

[30] G. Lampeas, V. Pasialis, X. Lin, E.A. Patterson, On the validation of solid mechanics models using optical measurements and data decomposition, Simul. Model. Pract. Theory. 52 (2015) 92–107. doi:10.1016/j.simpat.2014.12.006.

[31] E.. Hack, G.. Lampeas, E.A.. Patterson, An evaluation of a protocol for the validation of computational solid mechanics models, J. Strain Anal. Eng. Des. 51 (2016) 5–13. doi:10.1177/0309324715616017.

[32] C. Sebastian, E. Hack, E. Patterson, An approach to the validation of computational solid mechanics models for strain analysis, J. Strain Anal. Eng. Des. 48 (2012) 36–47. doi:10.1177/0309324712453409.

[33] R. Mukundan, S.H. Ong, P.A. Lee, Image analysis by Tchebichef moments, IEEE Trans. Image Process. 10 (2001) 1357–1364. doi:10.1109/83.941859.

[34] W. Wang, J.E. Mottershead, A. Ihle, T. Siebert, H.R. Schubach, Finite element model updating from full-field vibration measurement using digital image correlation, J. Sound Vib. 330 (2011) 1599–1620. doi:http://dx.doi.org/10.1016/j.jsv.2010.10.036.

[35] R.L.. Burguete, G.. Lampeas, J.E.. Mottershead, E.A.. Patterson, A.. Pipino, T.. Siebert, W.. f Wang, Analysis of displacement fields from a high-speed impact using shape descriptors, J. Strain Anal. Eng. Des. 49 (2014) 212–223. doi:10.1177/0309324713498074.

[36] W.J.R. Christian, E. Patterson, Euclid Ver: 1.01, (2018). http://www.experimentalstress.com/software.htm.

[37] P. Siegmann, L. Felipe-Sese, F. Diaz-Garrido, Improved 3D displacement measurements method and calibration of a combined fringe projection and 2D-DIC system, Opt. Lasers Eng. 88 (2017) 255–264. doi:10.1016/j.optlaseng.2016.08.014.

[38] E. López-Alba, F.A. Díaz-Garrido, Full-field indentation damage measurement using digital image correlation, Materials (Basel). 10 (2017). doi:10.3390/ma10070774.

[39] G. De Matteis, G. Brando, F.M. Mazzolani, Experimental and numerical analysis of pure aluminium shear panels for seismic protection of structures : An overview, 55 (2010).

[40] G.Y. Deng, C. Lu, L.H. Su, J.T. Li, H.T. Zhu, X.H. Liu, A.K. Tieu, A Study on the Aluminum Alloy AA1050 Severely Deformed by Non-Equal A study on the aluminum alloy AA1050 severely deformed by Non-equal channel angular pressing, (2013). doi:10.4028/www.scientific.net/AMR.651.442.

[41] H. Yu, C. Lu, K. Tieu, X. Liu, Y. Sun, Q. Yu, C. Kong, Asymmetric cryorolling for fabrication of nanostructural aluminum sheets, Sci. Rep. 2 (2012) 1–5. doi:10.1038/srep00772.